J Appl Electrochem (2007) 37:1129–1135
DOI 10.1007/s10800-007-9372-7

ORIGINAL PAPER

Preparation and characterization of $RuO_2 \cdot xH_2O$/carbon aerogel composites for supercapacitors

Jun Li · Xianyou Wang · Qinghua Huang · Chunling Dai · Sergio Gamboa · P. J. Sebastian

Received: 19 March 2007 / Revised: 9 July 2007 / Accepted: 9 July 2007 / Published online: 28 July 2007

Abstract A series of $RuO_2 \cdot xH_2O$/carbon aerogel (CA) composite electrode materials was prepared by a chemical precipitation method. Ultrasonication was used to accelerate the chemical reaction and improve the dispersion of $RuO_2 \cdot xH_2O$ particles on the surface and the pores of the aerogel. The structure and morphology of the as-prepared composite were characterized by N_2 adsorption isotherm, X-ray diffraction (XRD), and field emission-scanning electron microscopy (FE-SEM). The results showed that the CA had a pearly network structure and the composites had a relatively high specific surface area and mesopore volume. The electrochemical performance of the composite electrodes was studied by cyclic voltammetry, galvanostatic charge/discharge measurements and electrochemical impedance measurements. The results indicated a substantial increase in the specific capacitance of the composite. Moreover, the utilization efficiency of $RuO_2 \cdot xH_2O$ was greatly improved by loading it on the conductive and porous CA due to a significant improvement in the interparticle electronic conductivity and the extensive mesoporous network of the composites.

Keywords Carbon aerogel · $RuO_2 \cdot xH_2O$ · $RuO_2 \cdot xH_2O$/CA composite · Impregnation · Electrochemical properties

J. Li · X. Wang (✉) · Q. Huang · C. Dai
School of Chemistry, Xiangtan University, Hunan 411105, China
e-mail: wxianyou@yahoo.com

S. Gamboa · P. J. Sebastian
Solar-Hydrogen-Fuel Cell Group, CIE-UNAM, Temixco, Morelos 62580, Mexico

1 Introduction

Due to their high power density, excellent pulse charge-discharge properties and long cycle life, electrochemical supercapacitors have attracted considerable attention in many fields including surge-power delivery devices for electric vehicles, starting power for fuel cells, and backup-power storage for calculators and are also potential maintenance-free substitutes for batteries [1–3].

In supercapacitors energy is stored in terms of both double-layer capacitance and pseudocapacitance. The carbon materials with a high surface area are widely used for double layer capacitors, which utilize the capacitance arising from charge separation at an electrode/electrolyte interface. But this type of supercapacitor has limited energy capacity and power output. In order to enhance the energy density, researchers have made efforts to develop and modify carbonaceous materials by controlling the pore size distribution and introducing electroactive metallic particles or electroconducting polymers [4, 5]. Various forms of carbonaceous materials (activated carbon, carbon nanotubes, carbon nanofibre, and carbon aerogel) are used as candidates for the electrodes of supercapacitors [1, 2, 6]. Carbon aerogel (CA), a highly porous material, represents a promising and innovative material because of its attractive properties such as high electrical conductivity (25–100 S cm^{-1}), high porosity (80–98%), controllable pore structure and high surface area (up to 1,100 $m^2\ g^{-1}$) for double layer formation [6–8].

Redox supercapacitors utilize the charge-transfer pseudocapacitance arising from reversible Faradaic reactions occurring at the electrode/electrolyte interface. Transition metal oxides, such as hydrous RuO_2, NiO, and MnO_2, have been identified as possible electrode materials for high power and energy density supercapacitors [9–11].

The most widely investigated metal oxide is the amorphous form of hydrous ruthenium oxide ($RuO_2 \cdot xH_2O$), which displays a high specific capacitance (720 F g^{-1}) [11]. The advantages of $RuO_2 \cdot xH_2O$ include high specific capacitance, high conductivity, and excellent electrochemical reversibility. However, hydrous ruthenium oxide is very expensive. In order to reduce the cost of this material CNT-$RuO_2 \cdot xH_2O$ or AC-$RuO_2 \cdot xH_2O$ composite have been proposed as promising electrode materials in supercapacitors. The new electrode materials have much higher specific capacitance than other carbonaceous materials because they are based on a combination of double layer capacitance and Faradaic pseudocapacitance [11–13]. A ruthenium nanoparticle/CA composite was prepared via a novel impregnation method developed by Tamon et al. [14]. The resulting composite had highly dispersed Ru particles attached to the CA and was used as the electrode material for supercapacitors. Capacitances greater than 206 F g^{-1} were obtained for the samples with 35 wt.% Ru and the capacitance of these composites could be tailored by varying the Ru loading and/or the density of the host CA.

CA is a promising and innovative material for supercapactors, but it has generally been prepared under supercritical conditions. In our previous work [6, 7], we developed an ambient preparation technology for CA without supercritical conditions and studied its application for supercapacitors. In the present work $RuO_2 \cdot xH_2O$/CA composites were prepared by a chemical precipitation method. The electrochemical performances of CA and $RuO_2 \cdot xH_2O$/CA composite electrodes for the application of supercapacitors are investigated.

2 Experimental

2.1 Preparation of $RuO_2 \cdot xH_2O$/CA composite electrode

The CA was derived from pyrolysis of a resorcinol–formaldehyde (RF) gel. The molar ratio of formaldehyde to resorcinol was held at a constant value of two, Na_2CO_3 was used as the catalyst [6]. It was dissolved in distilled water, the mass percentage of the reactants in solution was set at RF = 40%, and the molar ratio of resorcinol (R) to catalyst (C) was set at R/C = 1,500. Sol–gel polymerization of the mixture was carried out in a sealed glass cylinder by holding the mixture at 333 K for 4 days. Acetone was selected as the drying solvent for ambient drying of the wet gels at 333 K for 4 days. RF gels were then dried completely under ambient conditions for 3 days. After drying, the CA was obtained by carbonization at 1,073 K for 3 h under a flow of pure Ar gas. The CA was treated in 2 M HNO_3 solution for 3 days. After filtration and washing with distilled water the CA was dried at a temperature of 100 °C.

Nanostructured composites with different $RuO_2 \cdot xH_2O$ loadings on CA were prepared by chemical precipitation. The required amount of CA was added to the $RuCl_3$ solution. Subsequently, 0.1 M NaOH was added slowly to the mixture to adjust the pH to a value of seven. During mixing, the solution was dispersed ultrasonically for 2 h to accelerate the reaction and improve the dispersion of $RuO_2 \cdot xH_2O$ particles on the surface of the CA. The black reaction product was filtered and washed repeatedly with distilled water. The resulting product was dried at a temperature of 423 K for 12 h in air. Then $RuO_2 \cdot xH_2O$/CA composites with different RuO_2 content (0, 10, 20, 30 wt.%) were obtained.

2.2 Structural characterization

The CA structures of CA and $RuO_2 \cdot xH_2O$/CA were determined by N_2 gas adsorption isotherm analysis at a temperature of 77 K on a Quantachrome autosorb automated gas sorption system (Version 1.17). The specific surface areas and pore size distributions were calculated using the Barrett–Joyner–Halenda (BJH) method.

X-ray diffraction (XRD) of CA and $RuO_2 \cdot xH_2O$/CA was performed on a diffractometer (D/MAX-3C) with Cu Kα radiation (λ = 1.54056 Å) and a graphite monochromator at 50 kV, 100 mA. The surface morphologies of CA and $RuO_2 \cdot xH_2O$/CA were examined using a field-emission scanning electron microscope (FE-SEM) performed on a Sirion 200.

2.3 Evaluation of electrochemical properties

The mass ratio of activated materials/graphite was 9:1. The powder mixture was mixed with 5 wt.% polytetrafluoroethylene (PTFE) (60%) used as a binder and kneaded to obtain a paste; the paste was pressed into the nickel foam substrate using a spatula, dried at 378 K for 12 h, and then pressed at 15 MPa for 1 min in order to assure good electrical contact.

The electrochemical properties of the obtained composite were studied with a three-electrode configuration consisting of a working electrode, a nickel sheet counter electrode and an Hg/HgO reference electrode at room temperature. The electrolyte was 6 M KOH. $RuO_2 \cdot xH_2O$/CA composites as electrode materials in supercapacitors were characterized using cyclic voltammetry (CV), a galvanostatic charge–discharge test and electrochemical impedance spectroscopy (EIS). The CV measurements were carried out at different scan rates in the voltage window –1.0–0 V. The dc charge/discharge tests were

carried out at constant current density of 5 mA g^{-1}. Electrochemical impedance spectroscopy (EIS) measurements were taken at ambient temperature in the frequency range 10 kHz–100 mHz using a frequency response analyzer (Solartron model 1260/1286, England).

3 Results and discussion

In order to investigate the morphology of CA and $RuO_2 \cdot xH_2O$/CA composites a direct morphological observation was conducted. High magnification FE-SEM images of CA and 30 wt.% $RuO_2 \cdot xH_2O$/CA composite are shown in Fig. 1. As seen in Fig. 1a the CA consists of a three-dimensional network of interconnected carbon particles and has an open structure with uniform particle size. Figure 1b shows that $RuO_2 \cdot xH_2O$ nanoparticles have deposited uniformly onto the surface of the porous CA and filled the inner large pores. The improvement in homogeneity is attributable to the pearly network structure of CA. At the higher scale image of the composite (Fig. 1c), a nano-network structure can also be seen. This indicates that the $RuO_2 \cdot xH_2O$ only impregnates along the pore walls of the CA and does not block the structure of the host CA.

Typical XRD patterns for CA and $RuO_2 \cdot xH_2O$/CA are presented in Fig. 2. Figure 2a shows strong carbon (002) and weak carbon (101) diffraction lines at 2θ (Cu Kα) of 22.0° and 44.0°, respectively. The CA can be regarded as partly graphitized carbon, though it differs from graphite. Hence, CA has high electrical conductivity. The XRD patterns for 30 wt.% $RuO_2 \cdot xH_2O$/CA are given in Fig. 2b. All patterns demonstrate that the $RuO_2 \cdot xH_2O$/CA composite has a poor crystalline structure; the intensities of the broad diffraction peaks corresponding to $RuO_2 \cdot xH_2O$ at 2θ of 28.6°, 36.6°, 55.8°, and 58.6°, are very low. These results indicate that the as-prepared composite has an amorphous structure. Also, although the $RuO_2 \cdot xH_2O$ is impregnated on the CA, the structure of the CA is not significantly influenced by the presence of $RuO_2 \cdot xH_2O$.

Physical adsorption of gases was carried out in order to characterize the porous structure of the samples. Figure 3 shows the typical N_2 adsorption/desorption isotherms at 77 K on the CA (Fig. 3a) and 30 wt.% $RuO_2 \cdot xH_2O$/CA (Fig. 3b). The adsorption and desorption isotherms of CA and $RuO_2 \cdot xH_2O$/CA are similar. According to the IUPAC recommendation, the two adsorption isotherms in Fig. 3 exhibit type IV characteristics, indicating that CA is a typical mesoporous material like RF aerogel. At low pressure micropore filling occurred. This indicates that some micropores exist in both the CA and the composite. At relative high pressures the isotherms have a hysteresis loop. Thus, the materials contain mesopores and show typical H1 characteristics attributable to cylindrical pores.

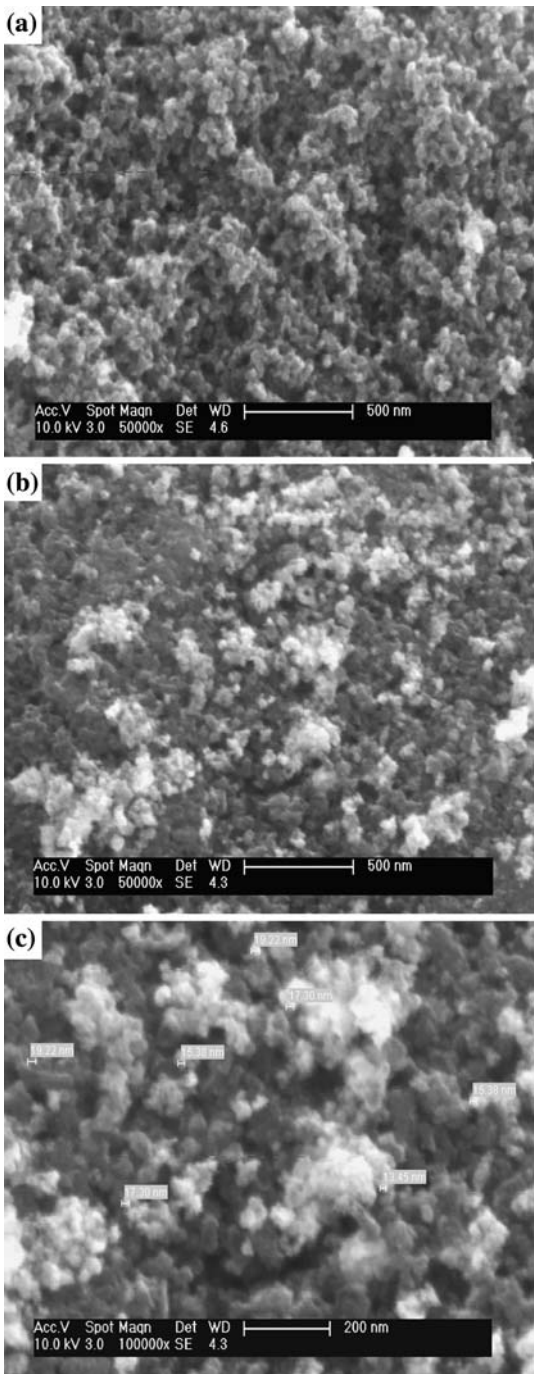

Fig. 1 High magnification FE-SEM images of CA (**a**) and 30 wt.% $RuO_2 \cdot xH_2O$/CA (**b**, **c**) composite

Hysteresis loops of isotherms are usually attributed to capillary condensation occurring in mesopores. The type H1 hysteresis loop observed for the samples is typical of pores in agglomerates of spheroidal particles of fairly uniform size and array [15]. The amount of N_2 adsorbed on the composite is smaller than that on the pure CA. The volume of adsorbed nitrogen has a tendency to decrease

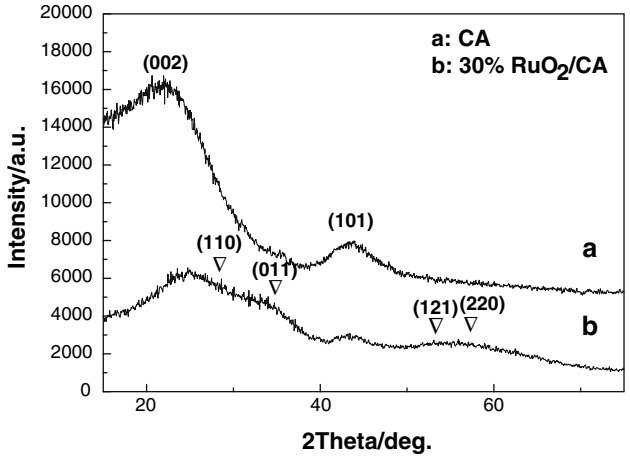

Fig. 2 XRD patterns for CA (**a**) and 30 wt.% $RuO_2 \cdot xH_2O$/CA (**b**) composite

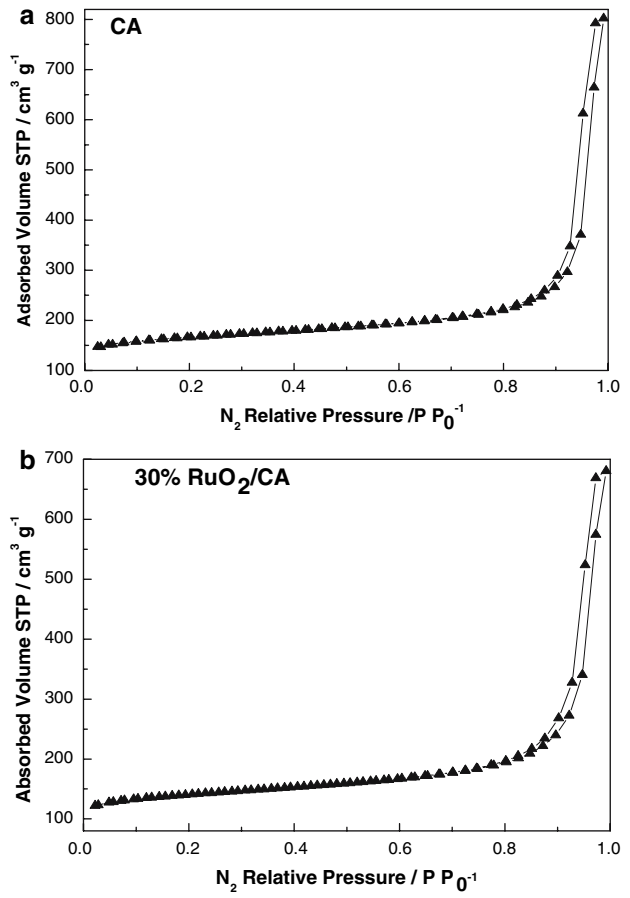

Fig. 3 Nitrogen adsorption isotherms at 77 K for samples (**a**) CA, (**b**) 30 wt.% $RuO_2 \cdot xH_2O$/CA

with $RuO_2 \cdot xH_2O$ insertion. However, the shapes of the N_2 adsorption isotherms for the composite and the CA are identical, indicating that the open mesoporous network of CA is maintained after the deposition of $RuO_2 \cdot xH_2O$. Due to this open network, ion accessibility from the electrolyte to the active mass of the $RuO_2 \cdot xH_2O$/CA composite should be favored; in addition, the advantage of the good electrical conductivity provided by the CA is maintained in the composite.

Figure 4 shows the pore size distribution, which was obtained from the N_2 sorption isotherms presented in Fig. 3 by the BJH method. Based on the definition from IUPAC, pores are classified into three groups: micropores (pore size < 2 nm), mesopores (2–50 nm), and macropores (>50 nm). The results in Fig. 4 confirm that the pores of the CA (Fig. 4a) and $RuO_2 \cdot xH_2O$/CA composite (Fig. 4b) are principally mesoporous. Thus, the CA and composite are theoretically suitable for supercapacitor materials due to the abundance of mesopores.

The textural parameters of CA and 30% $RuO_2 \cdot xH_2O$/CA calculated from the isotherm data are summarized in Table 1. The surface areas were determined by the BET

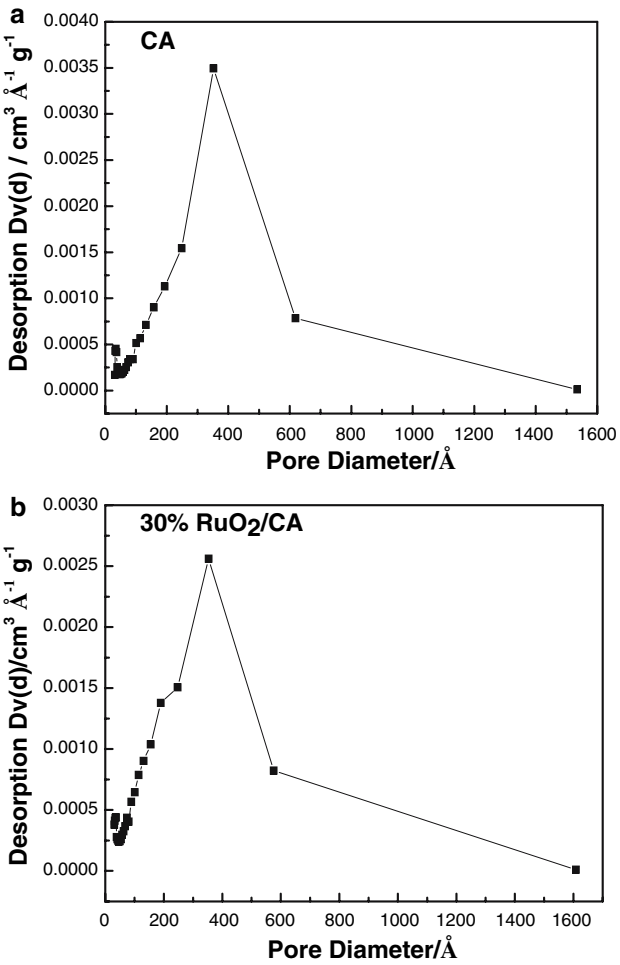

Fig. 4 Pore size distributions of CA (**a**), 30 wt.% $RuO_2 \cdot xH_2O$/CA (**b**)

Table 1 The textural parameters of CA and 30 wt.% $RuO_2 \cdot xH_2O$/CA

Samples	BET surface (Area/m^2 g^{-1})	Pore size (nm)	Pore volume (cm^3 g^{-1})	Micro pore volume (cm^3 g^{-1})
CA	626.40	7.92	1.24	0.29
30% RuO_2/CA	528.20	7.97	1.05	0.22

equation from the N_2 adsorption isotherm. The total pore volume was calculated from application of the Dubinin–Radushkevich (DR) equation to N_2 adsorption. The data in Table 1 show that both materials show similar characteristics, indicating that the CA structure is slightly affected by the $RuO_2 \cdot xH_2O$ nanoparticle impregnation. The pore volume and BET specific surface areas seem to decrease with RuO_2 impregnation due to blockage of micropores in the composite by RuO_2 nanoparticles. However, it is apparent that an extensive mesoporous network is still present in the composite. Therefore, it is anticipated that the composite could display good electrochemical properties because of its high BET surface area and mesopore volume.

Cyclic voltammograms for the $RuO_2 \cdot xH_2O$/CA composite electrodes (vs. Hg/HgO) at a scan rate of 2 mV s^{-1} are shown in Fig. 5. Both the pure CA electrode and the composite electrodes impregnated by different RuO_2 content exhibit good electrochemical behavior in Fig. 5. The CV profiles of the electrodes in Fig. 5 have rectangular-like shapes, indicating that the charging/discharging process of the $RuO_2 \cdot xH_2O$/CA composite electrode is reversible. In addition, the current increases proportionally with increasing $RuO_2 \cdot xH_2O$ loading, which suggests that there is a beneficial effect of $RuO_2 \cdot xH_2O$ loading. CV curves of $RuO_2 \cdot xH_2O$/CA composites are different from that of the

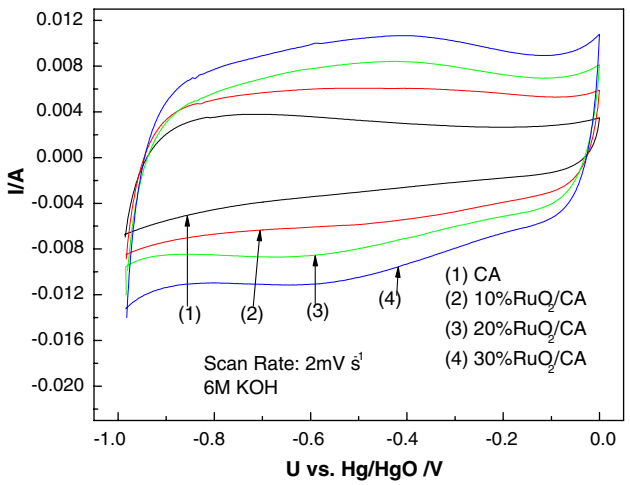

Fig. 5 Cyclic voltammograms for the $RuO_2 \cdot xH_2O$/CA composite electrodes at a scan rate of 2 mV s^{-1}

CA due to a Faradaic reaction of $RuO_2 \cdot xH_2O$ as follows [16]:

$$RuO_{(x+\delta)}(H_2O)_{(y-\delta)} + \delta e + \delta H_2O \rightarrow RuO_x(H_2O)_y \cdot \delta H_{ads.} + \delta OH^- \quad (1)$$

It is also evident that the mesoporous structure of the CA provides a very efficient environment for the well-dispersed impregnation of $RuO_2 \cdot xH_2O$ nanoparticles. When highly porous CA is impregnated with $RuO_2 \cdot xH_2O$ nanoparticles to form composite, the amount of absorbed electrolyte in the composite apparently increases. The contact area between the aqueous electrolyte and the $RuO_2 \cdot xH_2O$ nanoparticles increases due to the surface properties (hydrophilic or hydrophobic) of CA. As CA with high conductivity acts as a good current collector, the inter-particle electronic conductivity of the composite is significantly promoted. Moreover, the electrons from the Faradaic reaction of $RuO_2 \cdot xH_2O$ are extracted efficiently and rapidly [17–19]. Therefore, the capacitances of $RuO_2 \cdot xH_2O$/CA composite electrodes are larger than that of the CA based on double layer capacitance.

To analyze the variation of capacitance with the increase of the $RuO_2 \cdot xH_2O$ loading, the CV curves were measured in 6 M KOH. The specific capacitance of the electrodes can be estimated from the following equation [6]:

$$C_{s.t} = \frac{I_a + |I_c|}{2W(dV/dt)} \quad (2)$$

where I_a, I_c, W, and dV/dt are the sum of anodic and cathodic voltammetric currents on positive and negative sweeps, A; mass of the composite, g; the sweep rate, V s^{-1}, respectively.

The specific capacitance of $RuO_2 \cdot xH_2O$/CA composites in different scan rates based on the CV curves is presented in Fig. 6. As the scan rate increases the specific capacitance of the composite electrode gradually increases. When the $RuO_2 \cdot xH_2O$ content changes from 0 to 30 wt.%, the specific capacitance of the electrode increases dramatically, the capacitance for 30 wt.% $RuO_2 \cdot xH_2O$/CA composite is up to 386 F g^{-1}, which is greater than that of composite electrode reported by references (206 F g^{-1}) [17–19]. This shows that the ordered mesoporous structure increases greatly the utilization of $RuO_2 \cdot xH_2O$, because

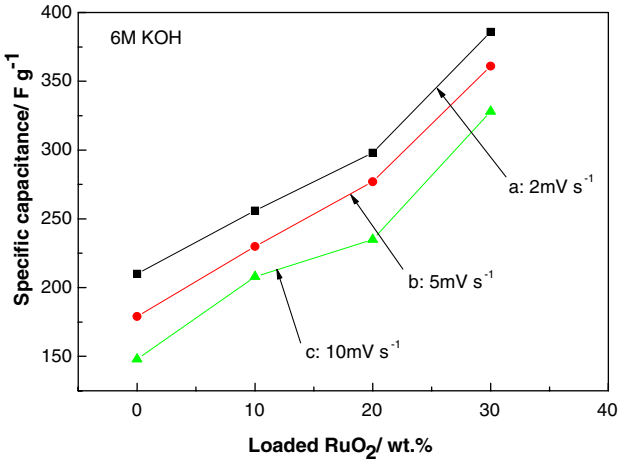

Fig. 6 The specific capacitance of $RuO_2 \cdot xH_2O$/CA composite electrodes with different scan rates

the mesoporous structure provides more effective surface to create pseudocapacitance, while the pseudocapacitance of $RuO_2 \cdot xH_2O$/CA composite is combined with the double-layer capacitance of the CA.

In order to gain a further understanding on the electrochemical performance of $RuO_2 \cdot xH_2O$/CA composite, the charge/discharge curves of the electrodes in 6 M KOH at a constant current of 100 mA g^{-1} from 0 to 1.2 V are shown in Fig. 7. The CA electrode and the 30 wt.% $RuO_2 \cdot xH_2O$/CA composite electrode have stable electrochemical properties in 6 M KOH. The curves are almost linear and there is a sudden drop in potential at the beginning of charge and discharge associated with the ohmic resistance. In general, the *E–t* relationships on these chronopotentiograms are approximately linear, indicating that the

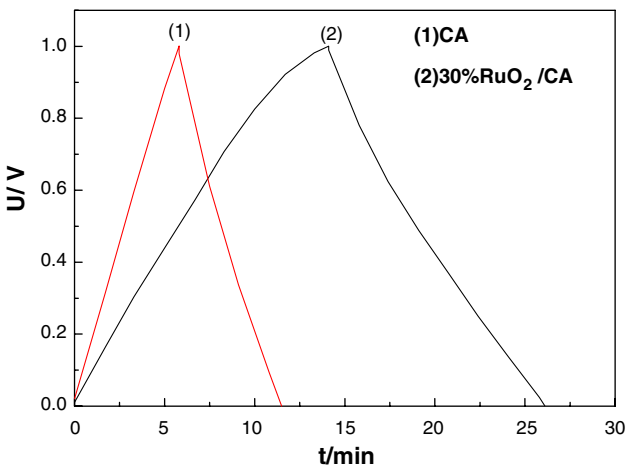

Fig. 7 The charge/discharge curves of electrodes measured in 6 M KOH at a constant current density of 100 mA g^{-1} from 0 to 1.2 V

$RuO_2 \cdot xH_2O$/CA electrodes behave as capacitors and give high values of charge/discharge efficiency.

The specific capacitance of the supercapacitor can be calculated by the following equation [6]:

$$C = 2 \times \frac{Q}{mV} = 2 \times 3600 \times 0.001 \times \frac{C^*}{mV} = 7.2 \times \frac{C^*}{mV} \quad (3)$$

where C is the specific capacitance of the supercapacitor, F g^{-1}; Q is electric quantity of the supercapacitor; C, C^* is the capacitance measured, mA h; m is the weight of a single electrode, g; V is the range of the charge/discharge, V.

Based on the experimental results of Fig. 7, it can calculated from Eq. 3 that the specific capacitance of a supercapacitor with 30 wt.% $RuO_2 \cdot xH_2O$/CA composite as electrode material is 86 F g^{-1}. Moreover, this specific capacitance value is obviously higher than that of the pure CA supercapacitor (28 F g^{-1}) [6].

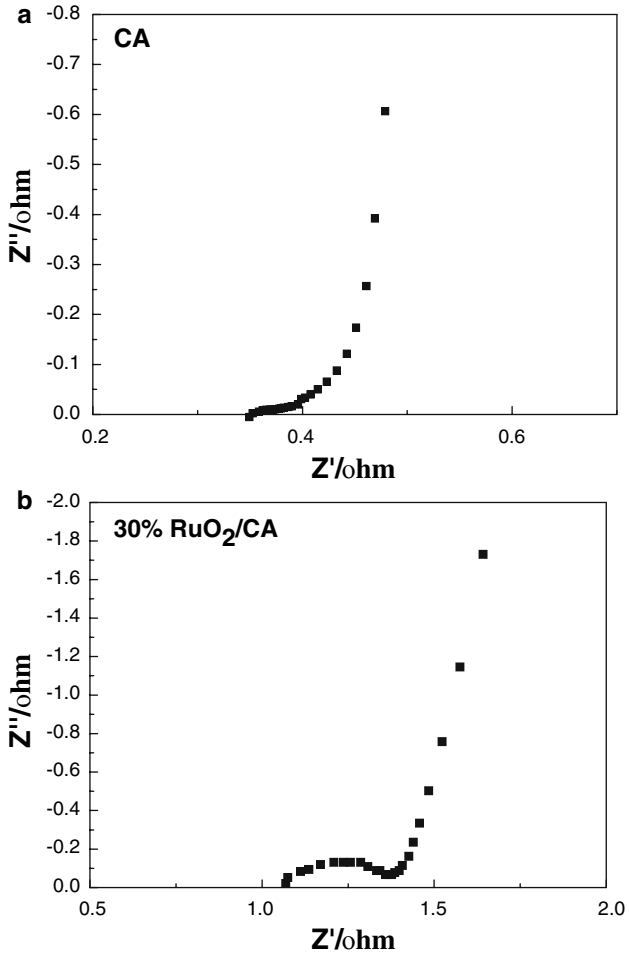

Fig. 8 Nyquist plots for the CA (**a**) and 30 wt.% $RuO_2 \cdot xH_2O$/CA composite (**b**) supercapacitors

Electrochemical impedance measurements are given in Fig. 8 in. In Fig. 8a, at low frequency, the CA electrode shows a vertical line showing an ideal capacitor behavior; at high frequency the impedance plot has a relatively small radius. In Fig. 8b, 30 wt.% $RuO_2 \cdot xH_2O$/CA composite electrode reveals a bigger semicircle than the CA electrode at high frequency, which may be explained by the Faradaic reaction. At lower frequency the impedance of the electrode increases and the plot deviates from ideal behavior, owing to the distributions of charge transfer rates, adsorption processes and redox reaction [20].

The diameter of the semicircle in impedance plots for porous materials is associated with pseudocapacitance and the porous structure of the material [18, 20]. From comparison of the impedance plots for CA electrode and the composite electrode in Fig. 8, it can be seen that the diameter of the semicircle increases with $RuO_2 \cdot xH_2O$ loading, indicating that the electrochemical reaction resistance of the composite electrode increases with $RuO_2 \cdot xH_2O$ impregnation. From the value of the point of intersection with the real axis in the high frequency range, the internal resistances of the CA and 30 wt.% $RuO_2 \cdot xH_2O$/CA composite are estimated to be 0.35 and 1.06 Ω, respectively. Apparently, lower resistance is beneficial for the application of supercapacitors. Therefore, the CA and composite, especially 30 wt.% $RuO_2 \cdot xH_2O$/CA composite, seem to be a promising active material for supercapacitors.

4 Conclusions

Various contents of $RuO_2 \cdot xH_2O$/CA composite electrode materials were synthesized by a chemical precipitation method. XRD and FE-SEM studies demonstrate that the CA is a partly graphitized amorphous material with a pearly network structure. N_2 adsorption isotherm measurements indicates that the open mesoporous network of the CA is maintained after impregnation of $RuO_2 \cdot xH_2O$. The composite has high BET surface area and mesopore volume. $RuO_2 \cdot xH_2O$/CA composites have stable electrochemical properties and excellent reversibility in 6 M KOH electrolytes. When the $RuO_2 \cdot xH_2O$ content is up to 30 wt.%, the specific capacitance of the electrode increases dramatically to 386 F g^{-1}. Therefore, impregnation of $RuO_2 \cdot xH_2O$ nanoparticle in the network structure of the CA improves electrochemical performance, and the ordered mesoporous structure of the CA increases the utilization of $RuO_2 \cdot xH_2O$. In addition, the composite has low resistance and good electrical conductivity. Thus, it can be concluded that a $RuO_2 \cdot xH_2O$/CA composite is a promising material for application in supercapacitors.

Acknowledgments This project was supported by the National Natural Science-Foundation of China under grant no. 50472080 and 20673092, Natural Science Foundation of Hunan Province, China under grant no. 04JJ3040, 05JJ20013, the Project of Nature Science Foundation of Jiangsu Province under the grant no. BK2003092 and DGAOA-UNAM (N102100), Mexico.

References

1. Emmenegger Ch, Mauron Ph, Sudan P, Wenger P, Hermann V, Gallay R, Züttel A (2003) J Power Sources 124:321
2. Frackowiak E, Lota G, Machnikowski J, Vix Guterl C, Beguin F (2006) Electrochim Acta 51:2209
3. Park BO, Lokhande CD, Park HS, Jung KD, Joo OS (2004) J Power Sources 134:148
4. Cottineau T, Toupin M, Delahaye T, Brousse T, Belanger D (2006) Appl Phys A-Mater A825:99
5. Kim C, Kim JS, Kim SJ, Lee WJ, Yang KS (2004) J Electrochem Soc 151:A769
6. Li J, Wang XY, Huang QH, Gamboa S, Sebastian PJ (2006) J Power Sources 158:784
7. Saquing CD, Kang D, Aindow M, Erkey C (2005) Micropor Mesopor Mater 80:11
8. Wu DC, Fu RW, Dresselhaus MS, Dresselhaus G (2006) Carbon 44:675
9. Wang GX, Zhang B, Yu ZL, Qu MZ (2005) Solid State Ionics 176:1169
10. Reddy RN, Reddy RG (2003) J Power Sources 124:330
11. Hu CC, Chen WC, Chang KH (2004) J Electrochem Soc 151:A281
12. Ramani M, Haran BS, White RE, Popov BN (2001) J Electrochem Soc 148:A374
13. Zheng JP (1999) Electrochem Solid ST 23:59
14. Tamon H, Ishizaka H, Yamamoto T, Suzuki T (1999) Carbon 37:2049
15. Raymundo-Pinero E, Khomenko V, Frackowiak E, Beguin F (2005) J Electrochem Soc 152:A229
16. Orena Y, Tamir A, Lederman Y, Gavra Z (2003) J Phys Chem Solids 64:1395
17. Park JH, Ko JM, Park O (2003) J Electrochem Soc 150:A864
18. Kim H, Popov BN (2002) J Power Sources 10:452
19. Sato Y, Yomogida K, Nanaumi T, Kobaykawa K, Ohsawa Y, Kawai M (2000) Electrochem Solid ST 3:113
20. Kim C (2005) J Power Sources 142:382